OPTIMIZATION OF MULTIELEMENT AIRFOILS FOR MAXIMUM LIFT

14

Lawrence E. Olson
NASA Ames Research Center
and
Aeromechanics Laboratory
U. S. Army Aviation R & D Command

SUMMARY

Two theoretical methods are presented for optimizing multielement airfoils to obtain maximum lift. The analyses assume that the shapes of the various high-lift elements are fixed. The objective of the design procedures is then to determine the optimum location and/or deflection of the leading- and trailing-edge devices. The first analysis determines the optimum horizontal and vertical location and the deflection of a leading-edge slat. The structure of the flow field is calculated by iteratively coupling potential-flow and boundary-layer analysis. This design procedure does not require that flow separation effects be modeled. The second analysis determines the slat and flap deflection required to maximize the lift of a three-element airfoil. This approach requires that the effects of flow separation from one or more of the airfoil elements be taken into account. The theoretical results are in good agreement with results of a wind-tunnel test used to corroborate the predicted optimum slat and flap positions.

INTRODUCTION

To achieve acceptable takeoff and landing performance, modern fixed-wing aircraft typically use mechanical high-lift devices such as leading-edge slats and slotted flaps. An essential step in the development of high-lift wings is the determination of the position (horizontal location, vertical location, and deflection) of the slat and/or flaps required to maximize aerodynamic performance. Theoretical methods which predict the optimum position of slats and flaps for multicomponent airfoils are being developed to: (1) reduce the number of high-lift configurations which must be evaluated experimentally; (2) reduce substantially the amount of wind-tunnel testing required to optimize a multicomponent airfoil; and (3) insure that experimentally determined optimums are true optimums. Two criteria generally used to evaluate the performance of a high-lift airfoil are maximum lift coefficient ($C_{\ell_{max}}$) and maximum lift to drag ratio $(C_\ell/C_d)_{max}$ at a given lift coefficient. This paper addresses the problem of optimization for maximum lift. At present, drag is not considered a criterion in the theoretical optimization method because the drag of multielement airfoils cannot be predicted accurately.

Configuration optimization of multielement airfoils for maximum lift is separable into two general classes of problems. This classification depends on the level of sophistication required of the aerodynamic analysis to determine the structure of the flow field and to evaluate the airfoil performance. Configurations which can be optimized without modeling the effects of flow separation are called Class 1 design problems. Configuration optimization which requires that the effects of flow separation be modeled are called Class 2 problems. For Class 1 optimization, viscous effects are determined by an analysis based on laminar and turbulent boundary-layer flows on the various airfoil surfaces. This type of analysis is simpler, requires less computation effort, and is generally more reliable than the separated flow modeling techniques required for Class 2 problems.

Section I outlines the aerodynamic analysis including a brief description of the separated flow model. The Class 1 design procedure is then used in Section II to determine the optimum position of a leading-edge slat. Optimization of the deflection angles of a slat and of a slotted flap for a three-element configuration is presented as a Class 2 design problem in Section III. Section IV briefly describes the experimental study conducted to obtain data for verification of the analysis techniques presented in this paper, and Section V compares theory with experiment for both optimization methods.

SYMBOLS

A wing area = cb

AR wing aspect ratio = b^2/A

b wing span

c airfoil reference chord = 1.7 m

C_d section drag coefficient = $\dfrac{\text{airfoil drag}}{(1/2)\ \rho_\infty U_\infty^2 c}$

C_f skin-friction coefficient at the upper surface trailing edge of airfoil component

C_ℓ airfoil lift coefficient = $\dfrac{\text{airfoil lift}}{(1/2)\ \rho_\infty U_\infty^2 c}$

C_L wing lift coefficient = $\dfrac{\text{wing lift}}{(1/2)\ \rho_\infty U_\infty^2 A}$

C_p airfoil surface pressure coefficient = $\dfrac{p-p_\infty}{(1/2)\ \rho U_\infty^2}$

p static pressure

Re reference chord Reynolds number = $\dfrac{U_\infty c}{\nu}$

s	chordwise distance along airfoil surface (measured from stagnation point)
s^*	dimensionless distance from separation point (eq. (6))
u	s-direction velocity component at outer edge of boundary layer
U_∞	free-stream velocity
v	velocity component normal to airfoil surface
x,y	horizontal and vertical coordinates in coordinate system of main airfoil
α	angle of attack, deg
δ	component deflection, deg
ν	kinematic viscosity
ρ	fluid density
τ_w	wall shear stress

Subscripts:

f	flap
m	main element
s	slat
∞	free stream

I. AERODYNAMIC ANALYSIS

General Comments

The objective of the theoretical analysis is to determine the position of a high-lift element (or elements) required to achieve maximum lift. Up to three design variables are required to specify position of each element. These position variables plus the angle of attack of the overall configuration result in a multidimension design space which is searched to determine the optimum position. As a result, not only must the aerodynamic analysis accurately predict the flow-field structure for a wide variety of configurations, but it must also be computationally efficient if the optimization technique is to be a useful design tool. It should be noted that the primary objective of the theoretical analysis is to determine the position of a high-lift element (or elements) required to achieve maximum lift.

Although the present analysis should give a reasonable estimate of the maximum lift coefficient of an optimized configuration, a more accurate computation of $C_{\ell_{max}}$ will be the subject of future study.

Potential-Flow Calculation

The potential-flow calculation is a singularity method where each of the airfoil contours (fig. 1) is represented by a large number (from 40 to 80) of straight line segments. A linear distribution of vorticity is placed on each of these segments. The present potential-flow analysis (ref. 1) not only provides the accurate surface pressure distributions required for subsequent boundary-layer analyses, but it is also computationally efficient. This efficiency is essential because a typical optimization calculation requires from 200 to 500 potential-flow solutions to complete the design procedure.

Boundary-Layer Analysis

The structure of the laminar, transitional, and turbulent boundary layers is calculated using the pressure field determined from the potential-flow analysis. For the three-element configuration considered in this study, a complete optimization calculation requires between 500 and 2000 solutions for conventional boundary layers such as those on the upper and lower surface of the leading-edge slat shown in figure 1. The need for computational efficiency resulted in the selection of the finite-difference method of Blottner (ref. 2) for solving the boundary-layer equations. The correlations of Smith (ref. 3) are used to determine the point of laminar instability. The transitional and turbulent boundary-layer eddy viscosity model of Cebeci (ref. 4) and Cebeci, Kaups, Mosinakis and Rehn (ref. 5) is then used to calculate Reynolds stresses. If laminar boundary-layer separation occurs, the empirical criteria of Gaster (ref. 6) is used to determine whether turbulent reattachment occurs. If reattachment is indicated, the calculation is continued as a turbulent boundary layer. If the criterion of Gaster indicates catastrophic flow separation, the boundary-layer calculation is terminated. A boundary-layer calculation of this type takes only 0.1 to 0.2 sec on the CDC 7600 computer.

The structure of the confluent boundary layer on the flap upper surface (fig. 1) is determined using the finite difference method of reference 7, a method which takes from 20 to 30 sec on the CDC 7600 computer for each confluent-boundary-layer calculation.

Potential-Flow/Boundary-Layer Coupling

The effect of boundary-layer displacement and entrainment on the inviscid flow is simulated by linear source distributions (fig. 1) placed on the straight line segments used to define the airfoil contours. The strength of the source distribution is equal to $d(u_e\delta^*)/ds$ where u_e is the velocity

at the edge of the boundary layer, δ^* is the local boundary-layer displacement thickness, and s is the arc length measured along the airfoil surface. This type of potential-flow/boundary-layer coupling is particularly useful when optimizing the position of high-lift devices because the displacement effect of any particular boundary layer can conveniently be "frozen." For example, the boundary layer on the lower surface of the flap (fig. 1) is not appreciably affected by changes in the leading-edge slat position. Therefore, the flap lower-surface boundary layer need only be computed for the initial slat position. The displacement effect for subsequent slat positions is then based on the flap lower-surface source strength distribution as calculated with the slate in the initial position.

Separated Flow Analysis

The separated flow model developed for the present study is similar to the source distribution method of Jacob and Steinbach (ref. 8). The separated flow model requires that the static pressure distributions in the separated zone (fig. 2) be nearly constant. This constant pressure condition in the separated region is approximated by requiring that the static pressure at s_2 (the central panel in the separated zone) and the the static pressure at s_3 (the trailing edge of the airfoil) both be equal to the static pressure at s_1 (the boundary-layer separation location). Thus

$$C_p(s_2) = C_p(s_1) \tag{1}$$

and

$$C_p(s_3) = C_p(s_1) \tag{2}$$

A two-parameter source distribution located on the surface of the airfoil in the separated zone (fig. 3) is introduced to enforce the above conditions. The functional form of the source distribution is given by

$$v = 2.5\, v_{max} s^* \qquad 0 \leq s^* \leq 0.4 \tag{3}$$

$$v = v_{max} \qquad 0.4 \leq s^* \leq 0.6 \tag{4}$$

$$v = v_{max} - (v_{max} - v_3)(5s^*-3)^2/4 \qquad 0.6 \leq s^* \leq 1.0 \tag{5}$$

where

$$s^* = (s - s_1)/(s_3 - s_1). \tag{6}$$

The separation location calculated from a previous iteration is used to determine the maximum source strength in the separated zone (v_{max}) and the

source strength at the airfoil trailing edge (v_3) so that equations (1) and (2) are satisfied. The airfoil static pressure distribution obtained from this solution is then used to recompute the airfoil upper-surface boundary layer and a new separation point is determined. This process is repeated until convergence is achieved.

Figure 4 compares the theoretically predicted lift for a range of angle of attack with experiment (ref. 9) for a GA(W)-1 airfoil. Figure 5 presents a similar comparison for a three-element configuration tested by Foster, Irwin, and Williams (ref. 10). The agreement between theory and experiment is good for both cases at angles of attack below stall. At angles of attack near stall the lift is underpredicted by approximately 8% for the GA(W)-1 airfoil and by 3% for the three-element configuration.

II. SLAT OPTIMIZATION: A CLASS 1 PROBLEM

The objective of this optimization procedure is to theoretically determine the position (horizontal location, vertical location, and deflection) of a leading-edge slat for maximum lift based on aerodynamic calculations which do not model the effect of flow separation. The analysis is based on the premise that, at the maximum lift coefficient at which attached flow can be maintained on the main airfoil, the optimum slat position for maximum lift minimizes the suction peak on the upper surface of the main element. For configurations which stall abruptly this is a reasonable assumption. However, for configurations which stall gradually, the validity of such an assumption remains to be proven.

The constrained function minimization method described by Vanderplaats in reference 11 and Vanderplaats and Moses (ref. 12) is used to numerically optimize the slat position so that the suction peak in the leading-edge region on the main component is minimized. This minimization is performed with the main element at a fixed angle of attack. The design variables (fig. 6) are slat horizontal and vertical location, and slat deflection. All three parameters are referenced to the slat trailing edge and can be varied independently.

Slat translation and deflection are subject to two constraints. The first constraint – that there be no flow separation on the slat upper surface – is applied to prevent the slat from moving into a separated flow regime. Numerically, this condition is satisfied by requiring that the skin-friction coefficient at the trailing edge of the upper surface of the slate, C_{f_s}, be slightly positive (i.e., $C_{f_s} \geq 0.0001$). The second constraint requires that the slat trailing edge be no closer than 0.02 c to the surface of main element (a reasonable slat gap for this configuration (ref. 10)). This constraint prevents the slat wake from merging with the boundary layer on the wing upper surface so that the computationally time consuming confluent boundary-layer calculation for the viscous flow above the main element can be replaced by a computationally efficient conventional boundary-layer calculation.

Figure 7 shows a sequence of positions through which the slat is moved during the numerical design procedure. For this particular example, the angle of attack of the main airfoil is 15°. With the slat in the initial position (slat position no. 1) it is lightly loaded, whereas the leading-edge region of the main airfoil is highly loaded, resulting in a large suction peak and a strong adverse pressure gradient. After nine iterations, each requiring the calculation of the gradient of the suction peak with respect to the three slat position variables, the analysis has converged and the slat position which minimizes the suction peak at an angle of attack of 15° has been determined. In this final position, the suction peak (and therefore the adverse pressure gradients on the main airfoil) has been substantially reduced in exchange for an increased loading on the slat. The numerical design thus yields a slat loading which is limited by the constraint that flow separation not occur on the slat upper surface. Figure 8 shows the surface pressure distributions for angles of attack of 13°, 19°, and 24° of the main airfoil. The slat position for all angles of attack is such that the suction peak is minimized and the slat upper-surface boundary layer is on the verge of separation.

Figure 9 shows the results of the analysis for a sequence of angles of attack from 13° to 24°. The figure shows the variation in slat horizontal position, slat vertical position and slat deflection as a function of angle of attack. Also shown is the skin-friction coefficient at the trailing edge of the upper surface of the main element, C_{f_m}. In figure 9, as the angle of attack is increased, the boundary layer on the main airfoil approaches separation (i.e., $C_{f_m} \to 0$). This separation is caused by an increase in the adverse pressure gradient on the main airfoil with angle of attack (see fig. 8) even though the slat is maintained in a position which minimizes the suction peak in the leading-edge region of the main component. Extrapolation of the numerical results predicts incipient flow separation ($C_{f_m} = 0$) on the main airfoil at an angle of attack of 24°. The slat position for this angle of attack is specified as the theoretically predicted optimum location required to give maximum lift, an assertion which will be verified by comparison with experiment.

III. SLAT/FLAP DEFLECTION OPTIMIZATION: A CLASS 2 PROBLEM

The objective of this optimization analysis is to determine the slat and flap deflections to obtain maximum lift for a three-element airfoil such as that shown in figure 10. The slat deflection is defined relative to a pivot point at the slat trailing edge. Thus the slat gap and slat overlap are independent of slat deflection. The pivot point for the flap is located on the flap upper surface directly below the wing trailing edge. Thus the flap gap and overlap are only weakly dependent on flap deflection. The optimum slat deflection and optimum flap deflection for maximum lift are determined by direct search relative to the two design variables, δ_s and δ_f. The effect of slat deflection and of flap deflection on computed $C_{\ell_{max}}$ is shown in figures 11 and 12, respectively. The slat gap for these calculations was 0.02 c and the flap gap was 0.03 c. These gaps are sufficiently large to insure that there is no strong interaction

between the wakes and the upper-surface boundary layers. It was also assumed, therefore, that the viscous flows on the upper surface of the main wing and flap could be analyzed as conventional boundary layers.

IV. EXPERIMENTAL OPTIMIZATION

As part of this study tests were conducted in the NASA Ames 40-by-80-Foot Wind Tunnel to experimentally determine optimum slat and flap positions for comparison with the theoretical predictions. The rectangular planform wing used in these tests (fig. 13) is equipped with a full-span leading-edge slat and a full-span single-slotted flap. The slat chord is 0.17 c and the flap chord is 0.40 c. The basic airfoil section is on RAE 2815. A detailed description of the slat, main airfoil, and flap shapes can be found in reference 10. The wing span is 16 m and the extended chord is 2.15 m. The relatively high aspect ratio of 7.5 and the rectangular planform result in a configuration with nearly two-dimensional flow over much of the wing span. Also, the use of a high aspect-ratio finite wing eliminates adverse wind-tunnel wall interference effects associated with two-dimensional high-lift airfoils which span the entire test section.

The slat and flap brackets permit continuous adjustment of the horizontal and vertical locations and the deflection of both elements. Data taken included lift using the wind-tunnel balance and surface static pressures along the model centerline. All data were obtained at a Reynolds number of 3.8×10^6 and a Mach number of 0.10.

V. COMPARISON OF THEORY AND EXPERIMENT

The experimentally and theoretically optimized slat positions are compared in figure 14 for a fixed flap deflection of 10°. The theoretical prediction is based on the Class 1 design procedure presented in Section II. It is to be noted that the largest differences between theory and experiment is 4° of slat deflection. The measured wing maximum lift coefficient with the slat in the theoretically optimized position differs only 4% from the experimentally measured maximum lift coefficient with the slat in the experimentally optimized position.

The comparison between theory and experiment for the slat/flap deflection optimization is summarized in figures 11 and 12. The experimentally measured maximum lift coefficient of the wing, $C_{L_{max}}$, is presented together with the wing centerline section maximum lift coefficient, $C_{\ell_{max}}$. The experimental value of $C_{\ell_{max}}$ was determined by correcting the measured $C_{L_{max}}$ for aspect ratio effects using the lifting line theory described by Glauert (ref. 13). The experimentally determined slat and flap deflections required to maximize the total wing lift are in good agreement with the optimum slat and flap deflections determined from the Class 2 analysis presented in Section III.

VI. CONCLUDING REMARKS

Optimization of multielement airfoils for maximum lift is separable into two general classes of problems. Class 1 problems are defined as those configurations which can be optimized using attached-flow, boundary-layer analysis. Class 2 design problems are defined as those which require the modeling of separated flows. A computationally efficient theoretical method for each class of problems is presented so that the position of leading- and trailing-edge high-lift devices can be optimized to obtain maximum lift. A Class 1 design procedure is described and applied to the optimization of the position of a leading-edge slat. A Class 2 analysis method is then described and applied to the optimization of the deflection of a leading-edge slat and a trailing-edge single-slotted flap to obtain maximum lift. In this investigation the effects of flow separation are modeled using surface source distributions located in the separated zones.

The theoretically optimized positions obtained from the Class 1 and Class 2 design procedures were then used as preliminary slat and/or flap positions for a wind-tunnel test of a three-element configuration. The refined optimum configurations derived from the wind-tunnel experiment are in good agreement with the theoretical results, indicating that both analysis methods are useful and reliable design tools.

REFERENCES

1. Olson, L. E.; and Dvorak, F. A.: Viscous/Potential Flow About Multi-Element Two-Dimensional and Infinite-Span Swept Wings: Theory and Experiment. AIAA Paper 76-18, AIAA 14th Aerospace Sciences Meeting, Washington, D. C., Jan. 26-28, 1976.

2. Blottner, F. G.: Variable Gird Scheme Applied to Turbulent Boundary Layers. Computer Methods in Appl. Mech. and Eng., vol. 4, Sept. 1974, pp. 179-194.

3. Smith, A. M. O.: Transition, Pressure Gradient and Stability Theory. Proc. 9th International Congress of Applied Mechanics, Brussels, vol. 7, 1957, pp. 234-244.

4. Cebeci, Tuncer: Calculation of the Three-Dimensional Boundary Layer I. Swept Infinite Cylinders and Small Cross Flow. AIAA J., vol. 12, no. 6, June 1974, pp. 779-786.

5. Cebeci, Tuncer; Kaups, Kalle; Mosinakis, G. J.; and Rehn, J. A.: Some Problems of Calculations of Three-Dimensional Boundary Layer Flows on General Configurations. McDonnell Douglas Report No. MDC J5884, April 1973.

6. Gaster, M.: The Structure and Behavior of Laminar Separation Bubbles. ARC 28-226, 1967.

7. Dvorak, F. A.; and Woodward, F. A.: A Viscous/Potential Flow Interaction Analysis Method for Multi-Element Infinite Swept Wings. vol. 1, NASA CR-2476, Nov. 1974.

8. Jacob, K., and Steinbach, D.: A Method for Prediction of Lift for Multi-Element Airfoils with Separation, AGARD-CP-143, V/STOL Aerodynamics, April 1974.

9. McGhee, Robert J.; and Beasley, William D.: Low-Speed Aerodynamic Characteristics of a 17-Percent-Thick Airfoil Section Designed For General Aviation Applications. NASA TN D-7428, 1973.

10. Foster, D. N., Irwin, H. P., and Williams, B. R.: The Two Dimensional Flow Around a Slotted Flap. RAE Tech. Report 70164, Sept. 1970.

11. Vanderplaats, Garret N.: CONMIN-A Fortran Program for Constrained Function Minimization. NASA TM X-62,282, 1973.

12. Vanderplaats, Garret N.; and Moses, Fred: Structural Optimization by Methods of Feasible Directions. Computers & Structures vol. 3, 1973, pp. 739-755.

13. Glauert, H.: The Elements of Aerofoil and Airscrew Theory. Cambridge at the University Press, 1948.

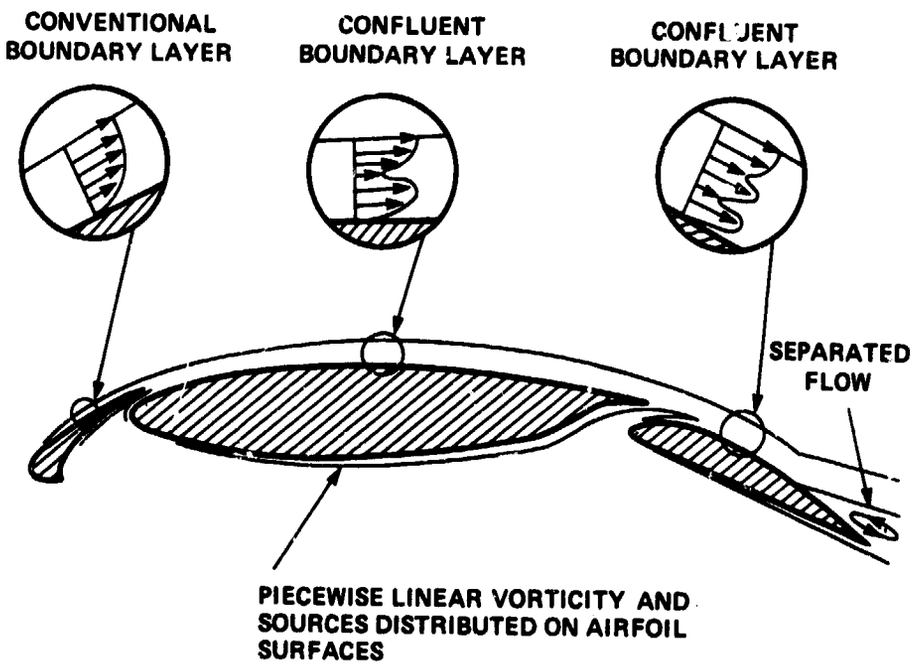

Figure 1.- Flow about multielement airfoil.

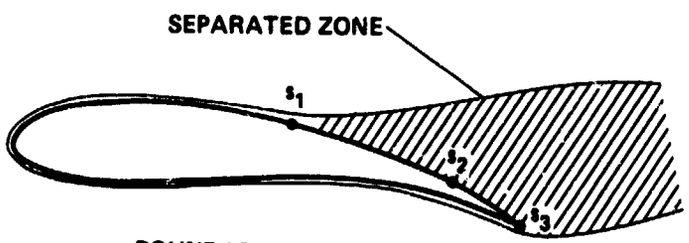

s_1 = BOUNDARY-LAYER SEPARATION POINT
s_2 = CENTER PANEL IN SEPARATED ZONE
s_3 = TRAILING EDGE OF AIRFOIL

REQUIRE: $C_p(\text{at } s_1) = C_p(\text{at } s_2) = C_p(\text{at } s_3)$

Figure 2.- Separated flow model.

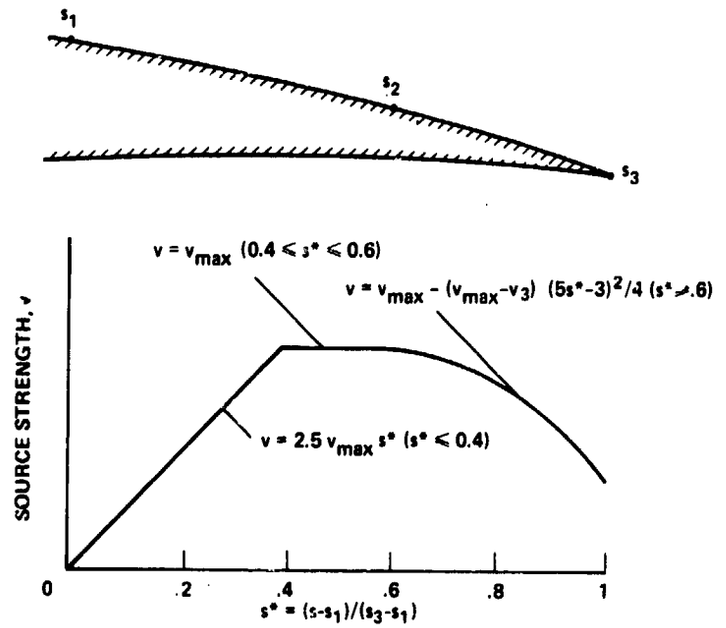

Figure 3.- Two-parameter source distribution in separated zone.

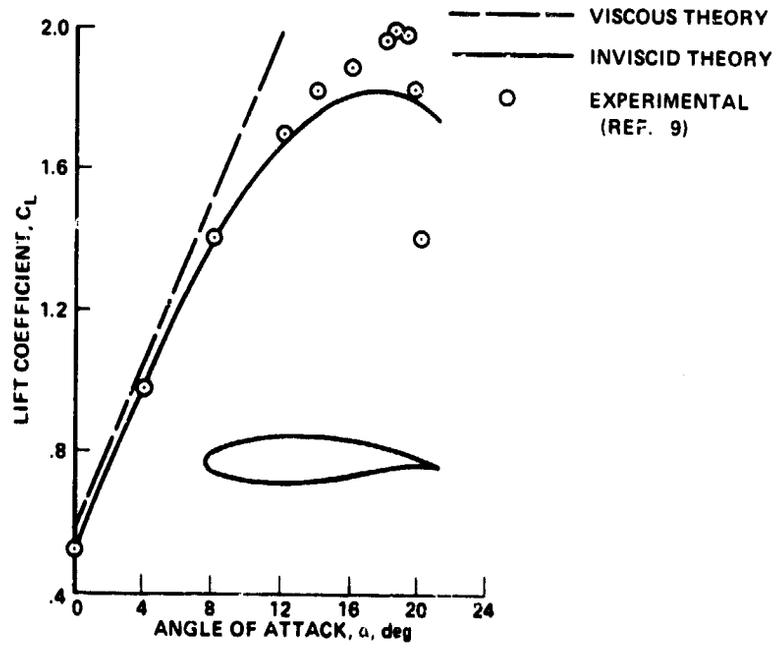

Figure 4.- Comparison of experimental and calculated lift on a GA(W)-1 airfoil. Re = 5.7×10^6; M = 0.15.

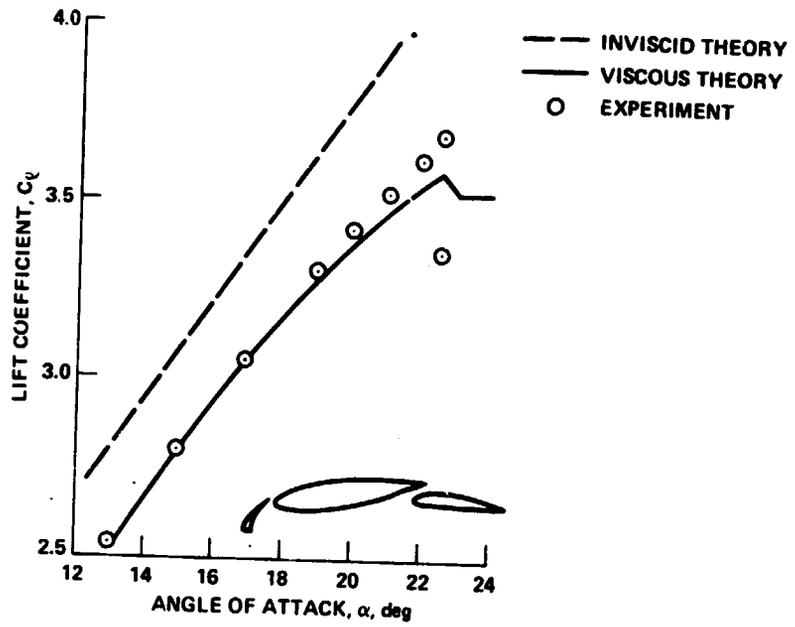

Figure 5.- Comparison of experimental and calculated lift on a three-element airfoil. Re = 3.8×10^6; M = 0.20.

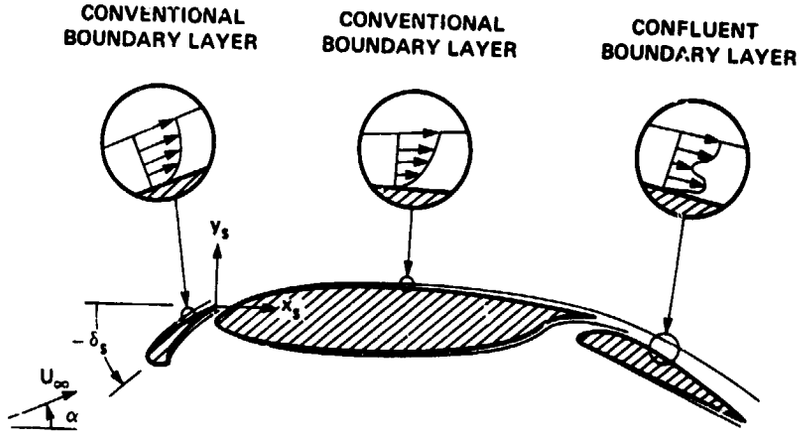

x_s = x-COORDINATE OF SLAT TRAILING EDGE
y_s = y-COORDINATE OF SLAT TRAILING EDGE
δ_s = SLAT DEFLECTION

} DESIGN VARIABLES

Figure 6.- Aerodynamic analysis for leading-edge slat-position optimization for maximum lift.

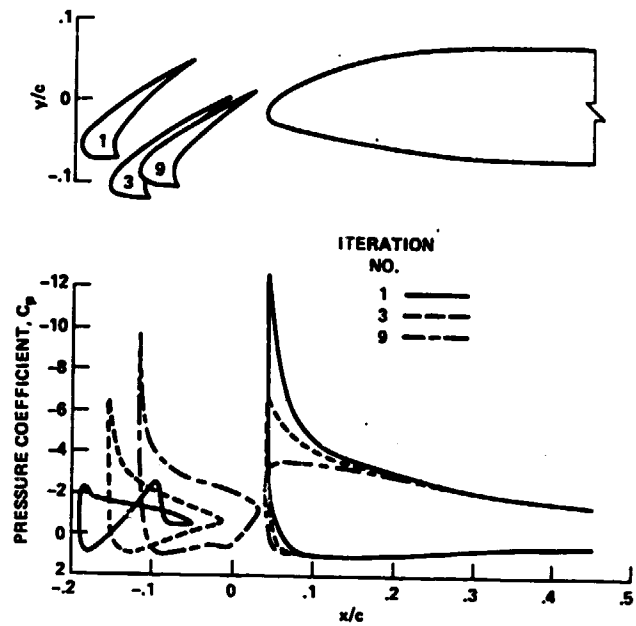

Figure 7.- Minimization of main airfoil suction peak at an angle of attack of 15°. δ_f = 10°; Re = 3.8 × 10^6; M = 0.10.

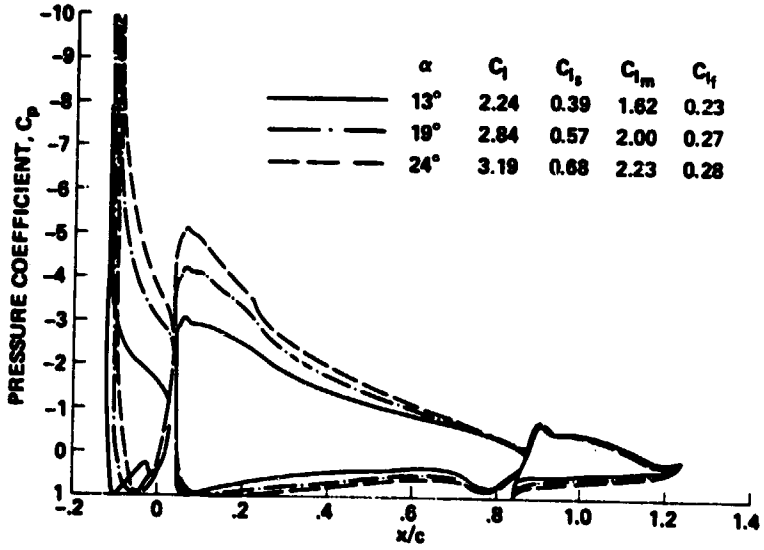

Figure 8.- Pressure distribution on a three-element airfoil with slat positioned to minimize the suction peak on the main airfoil. δ_f = 10°; Re = 3.8 × 10^6; M = 0.10.

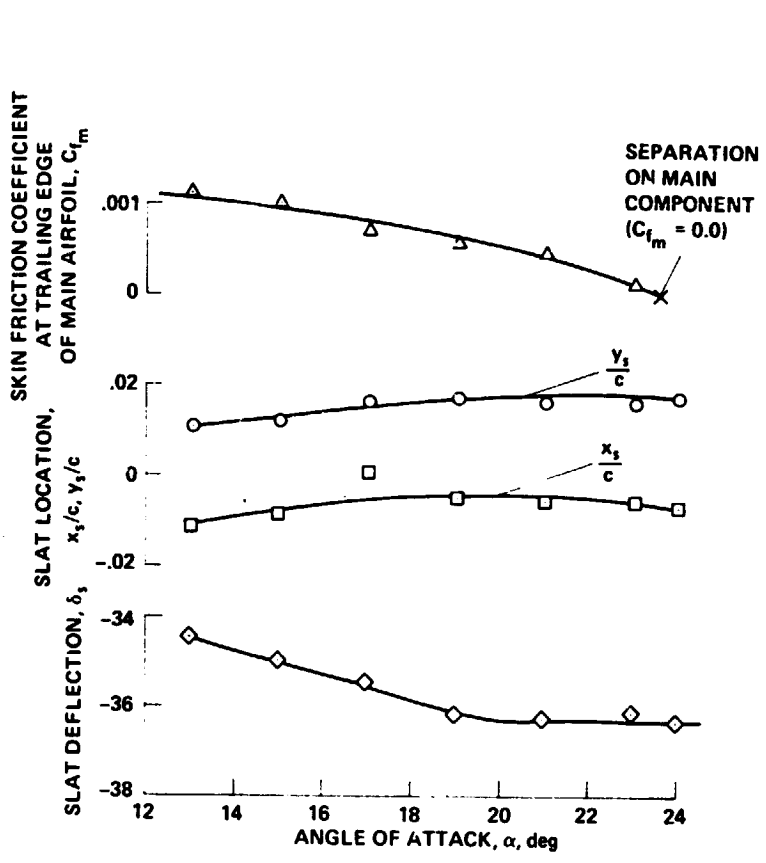

Figure 9.- Effect of configuration angle of attack on the skin-friction coefficient at the trailing edge of the main component and on the slat position required to minimize the suction peak on the main component. $\delta_f = 10^o$; Re = 3.8×10^6; M = 0.10.

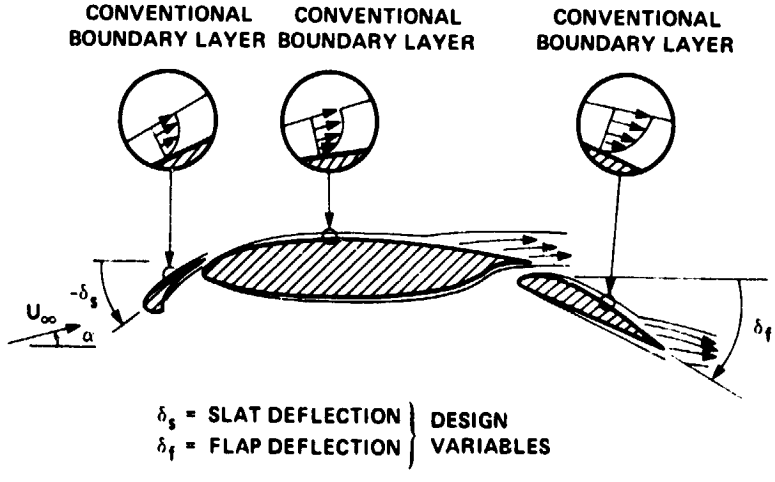

Figure 10.- Aerodynamic analysis for leading-edge slat and trailing-edge flap-deflection optimization for maximum lift.

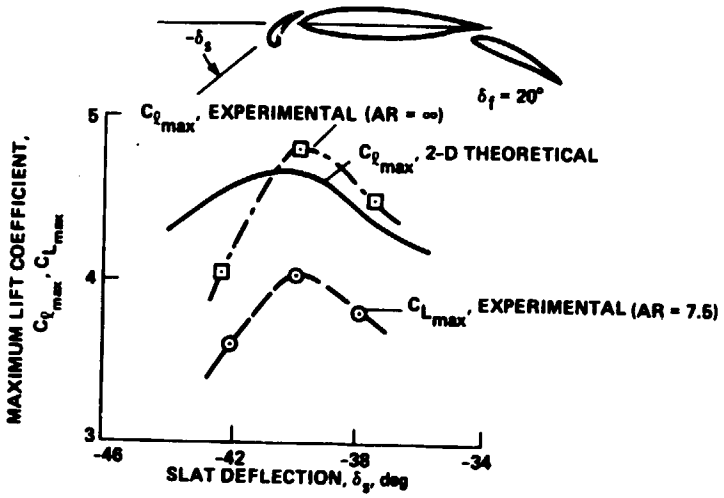

Figure 11.- Comparison of the effect of slat deflection on the computed maximum airfoil lift $C_{\ell_{max}}$ with the effect of slat deflection on the measured wing maximum lift $C_{L_{max}}$ for three-element configuration. Re = 3.8 × 10^6; M = 0.10.

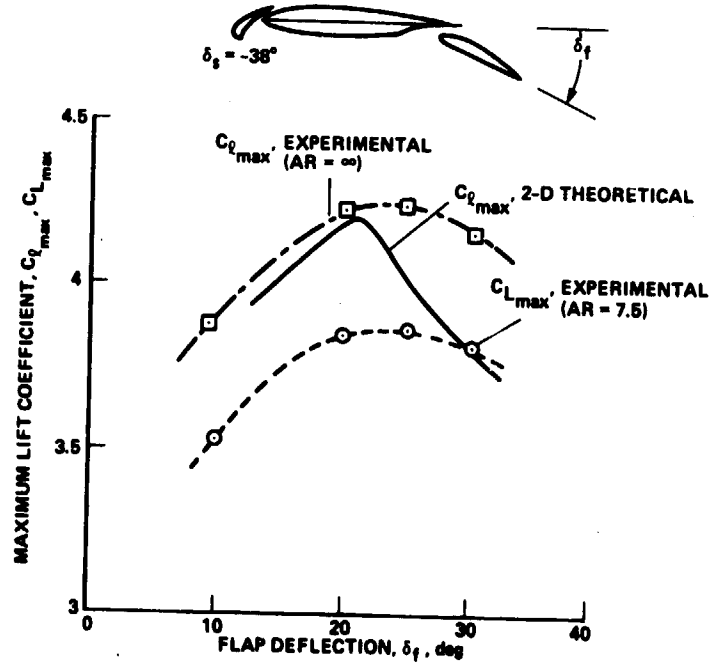

Figure 12.- Comparison of the effect of flap deflection on the computed maximum lift $C_{\ell_{max}}$ with the effect of flap deflection on the measured wing maximum lift $C_{L_{max}}$ for a three-element configuration. Re = 3.8 × 10^6; M = 0.10.

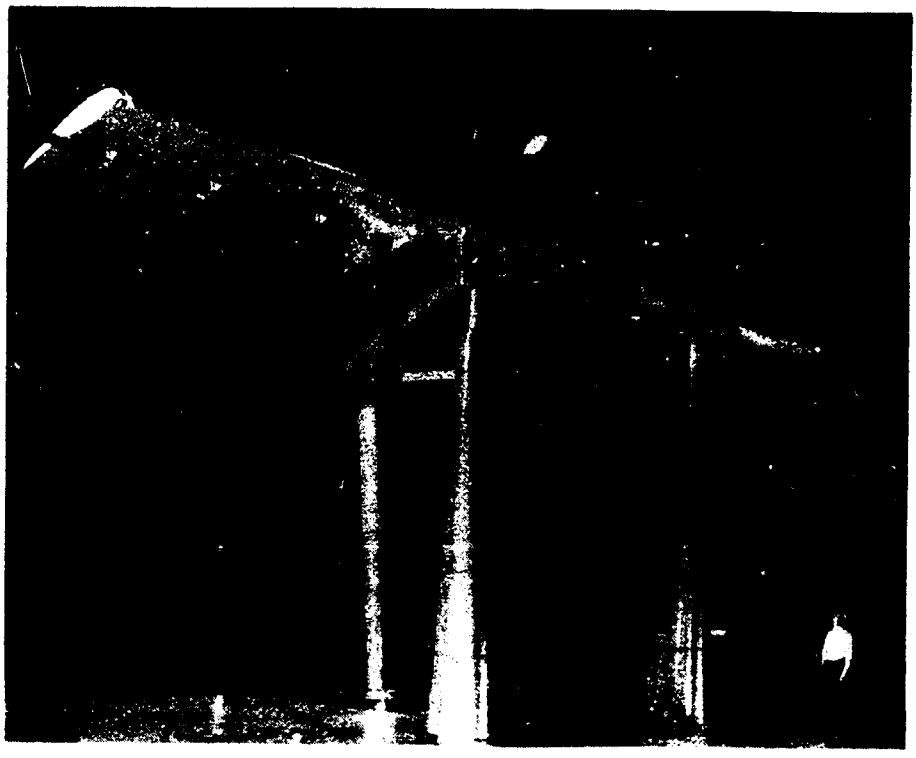

Figure 13.- Wind-tunnel model used to determine experimentally optimum slat and flap positions for maximum lift.

SLAT LOCATION	x_s/c	y_s/c	δ_s	$C_{L_{max}}$ (EXPERIMENTAL)
A	-0.007	0.017	-36	3.16
B	-0.009	0.010	-40	3.28

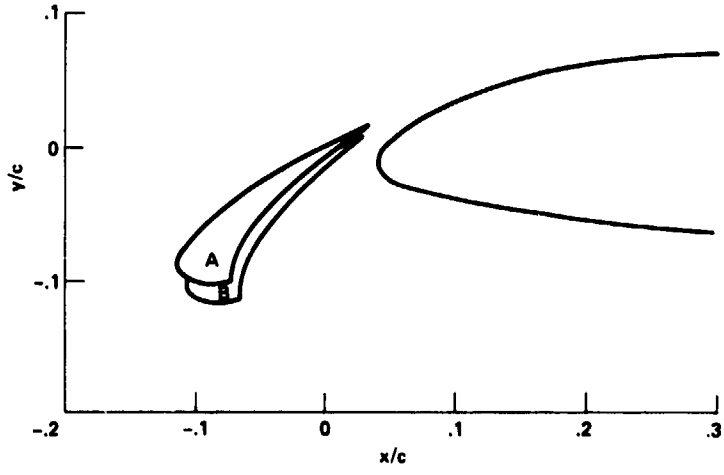

Figure 14.- Comparison of theoretically and experimentally optimized leading-edge slat position. Position A is theoretical; position B is experimental; $\delta_f = 10^o$; Re = 3.8×10^6.